ELSEVIER

The SPINE JOURNAL

The Spine Journal 000 (2022) 1–12

Basic Science

Innovative design of bone quality-targeted intervertebral spacer: accelerated functional fusion guiding oriented collagen and apatite microstructure without autologous bone graft

Aira Matsugaki, PhD[a,b], Manabu Ito, MD, PhD[c], Yoshiya Kobayashi, MEng[a], Tadaaki Matsuzaka, MEng[a], Ryosuke Ozasa, PhD[a,b], Takuya Ishimoto, PhD[a,b], Hiroyuki Takahashi, PhD[d], Ryota Watanabe, MEng[a,d], Takayuki Inoue, PhD[d], Katsuhiko Yokota, BA[d], Yoshio Nakashima, MEng[d], Takashi Kaito, MD, PhD[e], Seiji Okada, MD, PhD[e], Takao Hanawa, PhD[a,f], Yukihiro Matsuyama, MD, PhD[g], Morio Matsumoto, MD, PhD[h], Hiroshi Taneichi, MD, PhD[i], Takayoshi Nakano, PhD[a,b,*]

[a] *Division of Materials and Manufacturing Science, Graduate School of Engineering, Osaka University, 2-1, Yamada-Oka, Suita, Osaka, 565-0871, Japan*

[b] *Anisotropic Design and Additive Manufacturing Research Center, Osaka University, 2-1 Yamada-Oka, Suita, Osaka, 565-0871, Japan*

[c] *Department of Spine and Spinal Cord Disorders, National Hospital Organization, Hokkaido Medical Center,5-7-1-1, Yamanote, Nishi-ku, Sapporo, Hokkaido, 063-0005, Japan*

[d] *Teijin Nakashima Medical Co., Ltd., 688-1 Joto-Kitagata, Higashi-ku, Okayama, 709-0625, Japan*

[e] *Department of Orthopaedic Surgery, Osaka University Graduate School of Medicine, 2-2 Yamada-Oka, Suita, Osaka, 565-0871, Japan*

[f] *Institute of Biomaterials and Bioengineering, Tokyo Medical and Dental University, 2-3-10 Kanda-Surugadai, Chiyoda-ku, Tokyo, 101-0062, Japan*

[g] *Department of Orthopaedic Surgery, Hamamatsu University School of Medicine, 1-20-1 Handayama, Higashi-ku, Hamamatsu, Shizuoka, 431-3192, Japan*

[h] *Department of Orthopaedic Surgery, Keio University School of Medicine, 35 Shinano-machi, Shinjuku-ku, Tokyo, 160-8582, Japan*

[i] *Department of Orthopaedic Surgery, Dokkyo Medical University School of Medicine, 880 Kitakobayashi, Mibu, Tochigi, 321-0293, Japan*

Received 26 June 2022; revised 28 November 2022; accepted 7 December 2022

Abstract

BACKGROUND CONTEXT: Although autologous bone grafting is widely considered as an ideal source for interbody fusion, it still carries a risk of nonunion. The influence of the intervertebral device should not be overlooked. Requirements for artificial spinal devices are to join the vertebrae together and recover the original function of the spine rapidly. Ordered mineralization of apatite crystals on collagen accelerates bone functionalization during the healing process. Particularly, the stable spinal function requires the ingrowth of an ordered collagen and apatite matrix which mimics the intact intervertebral microstructure. This collagen and apatite ordering is

FDA device/drug status: Not applicable.

Author disclosures: ***AM:*** Nothing to disclose. ***MI:*** Nothing to disclose. ***YK:*** Nothing to disclose. ***TM:*** Nothing to disclose. ***RO:*** Nothing to disclose. ***TI:*** Nothing to disclose. ***HT:*** Nothing to disclose. ***RW:*** Nothing to disclose. ***TI:*** Nothing to disclose. ***KY:*** Nothing to disclose. ***YN:*** Nothing to disclose. ***TK:*** Nothing to disclose. ***SO:*** Nothing to disclose. ***TH:*** Nothing to disclose. ***YM:*** Nothing to disclose. ***MM:*** Nothing to disclose. ***HT:*** Nothing to disclose. ***TN:*** Grant: Japan Society for the Promotion of Science (JSPS) (H, Paid directly to institution). Grant: Japan Agency for Medical Research and Development (AMED) (F, Paid directly to institution).

*Corresponding author. Division of Materials and Manufacturing Science, Graduate School of Engineering, Osaka University, 2-1, Yamada-Oka, Suita, Osaka 565-0871, Japan. Tel.: +81 6 6879 7505.

E-mail address: nakano@mat.eng.osaka-u.ac.jp (T. Nakano).

https://doi.org/10.1016/j.spinee.2022.12.011

imperative for functional bone regeneration, which has not been achieved using classical autologous grafting.

PURPOSE: We developed an intervertebral body device to achieve high stability between the host bone and synthesized bone by controlling the ordered collagen and apatite microstructure.

STUDY DESIGN: This was an in vivo animal study.

METHODS: Intervertebral spacers with a through-pore grooved surface structure, referred to as a honeycomb tree structure, were produced using metal 3D printing. These spacers were implanted into normal sheep at the L2–L3 or L4–L5 disc levels. As a control group, grafting autologous bone was embedded. The mechanical integrity of the spacer/bone interface was evaluated through push-out tests.

RESULTS: The spacer with honeycomb tree structure induced anisotropic trabecular bone growth with textured collagen and apatite orientation in the through-pore and groove directions. The push-out load of the spacer was significantly higher than that of the conventional autologous graft spacer. Moreover, the load was significantly correlated with the anisotropic texture of the newly formed bone matrix.

CONCLUSIONS: The developed intervertebral spacer guided the regenerated bone matrix orientation of collagen and apatite, resulting in greater strength at the spacer/host bone interface than that obtained using a conventional gold-standard autologous bone graft.

CLINICAL SIGNIFICANCE: Our results provide a foundation for designing future spacers for interbody fusion in human.

Keywords: Bone quality; Collagen and apatite orientation; Intervertebral spacer; Push-out strength; Spinal fusion; Through-pore grooved surface structure

Introduction

In spinal fusion surgery, adjacent vertebrae must be immobilized via tight joints. The gold standard for bone-forming treatment is autogenous iliac crest bone autograft [1,2]. Although surgery is widely performed for spine regeneration, improved methods are needed to avoid revision surgery and painful postoperative complications. Using structured biomaterials as synthetic grafts is advantageous compared with using autogenic grafts because of the ability of synthetic materials to stimulate osteoconduction [3,4]. Importantly, when using synthetic graft materials for spinal fusion, the cell/device interface can actively mediate osteoconduction during the initial period of bone regeneration and during long-term stabilization. Moreover, the regeneration process does not require initial resorption of the grafted bone, enabling rapid fusion and functionalization of the vertebrae.

The spine provides mechanical support and houses the spinal cord and nerves. The mechanical functionalization of bone, including the vertebrae, is governed by not only the bone mass, but also the crystallographic texture of apatite, which is among the most important bone quality factors [5,6]. Apatite is oriented in the same direction as collagen fibers in intact bone [7], and the collagen and apatite bone matrix anisotropy varies depending on the anatomical region [8,9]. This anisotropy is strictly facilitated by the surrounding mechanical condition [10]. In several bone diseases, deterioration in the anisotropy of collagen and apatite texturization leads to severe pathological bone dysfunction, including rheumatic arthritis [11], osteoporosis [12], and tumorigenesis [13,14]. Importantly, bone matrix texturization takes much longer than bone mass recovery because immaturely massed bone cannot experience enough mechanical loading stimuli [15]. Long-term stabilization of the host bone and regenerated bone cannot be achieved until the crystallographic texture of both the original host bone and new bone is ordered in the same direction. For example, the surface structure of hip implants promotes anisotropy in the regenerated bone microstructure by mediating consistent loading stress from the host bone [16]. Anisotropic connectivity through the host bone and regenerated bone determines the success or failure of bone replacement surgery. This anisotropic relationship mediated by the intervertebral body is crucial for successful fusion and prevents loosening in spinal fusion, which requires not only a physical connection but also innate structural recovery, including formation of the oriented collagen and apatite microstructure [5,6]. Spine vertebrae exhibit a characteristic hierarchically anisotropic microstructure in which trabecular bones run along the cephalocaudal axis [17] and a further nanometer-scale micro-arrangement of collagen and apatite runs along the trabecular long axis. This structural anisotropy strengthens the mechanical properties along the cephalocaudal axis [5,6]. To generate a hierarchical anisotropic bone micro-arrangement, the texture of the newly formed bone must be artificially controlled immediately after implantation. The development of designed spacers for textural control of intervertebral bodies may enable stable spinal fusion, which would eliminate the need for secondary surgeries and reduce financial and mental burdens to patients.

Collagen and apatite from the initial regeneration stage becomes organized when the individual cells that produce the bone matrix are aligned, as described in our previous studies [18–20]. Particularly, a unidirectional patterned surface guides the anisotropic microstructure of the collagen and apatite bone matrix [21,22]. The deposition

pathway of anisotropic bone matrix is strictly regulated by the nucleation and transport systems of collagen fibrils [23]. Elongated cells produce vesicles for collagen deposition, and oriented fibrogenesis occurs outside of cells. We proposed using an intervertebral spacer with our original honeycomb tree structure (HTS) design [24]. We previously demonstrated the advantage of our designed HTS using an embedded cage model within the vertebral body. The environment surrounding the intervertebral body is regulated by its avascular nature, which exhibits a different metabolic condition and mechanical environment from those inside the vertebral body. Blood and nutrient supplies are limited in the intervertebral space compared with those inside the vertebral bodies [25]. In clinical settings, embedding of the spacers between the vertebrae is essential, which was lacking in our previous work.

In the current study, we evaluated the spinal fusion activity of HTS by using a newly developed intervertebral fusion model. A strictly designed unidirectional groove microstructure can guide cell alignment even without mechanical loading in the early stages of bone regeneration. The loading stimuli can act as potential regulators of stress-induced bone texturization. Metal 3D printing technology can be used to generate an HTS structure that does not require autologous bone grafting or secondary surgery, providing new approaches for spinal fusion therapy.

Materials and methods

Design of an intervertebral spacer

To achieve osteoblast alignment and ensure the subsequent preferential orientation of the collagen and apatite bone matrix, an intervertebral spacer with an internal HTS [24] was modeled using computer-aided design. The HTS had the following characteristics:

(1) Unidirectional through-pores were aligned along the height direction of the spacer.

(2) Unidirectional grooves parallel to the through-pore direction were located on the pore surface. The periodicity (bottom-to-bottom distance between neighboring grooves) was 400 μm.

(3) The cross-section of the pore was an equilateral triangle with a gap in fluid circulation. The triangle was inscribed by a circle with a diameter of 1 mm.

The HTS can be described as “a through-pore with a grooved substrate” that elongates in one direction (height direction of the spacer).

The spacer was composed of solid walls on the sides and had windows to ensure fluid circulation between the inside and outside of the spacer (Fig. 1). The outer shape of the spacer was a box-type. As a control, we modeled a spacer with an identical outer shape but a large space in the center for grafting autologous bone, which can be adapted to many conventional spacers. The space dimensions were determined such that the projected area of the opening (white regions in Fig. 1(B) and 1(C)) was equivalent to that of our designed spacer. No autologous bone was implanted in the novel spacer.

Fabrication of intervertebral spacer using 3D printer

Based on the computer-aided design model, intervertebral spacers were produced from Ti-6Al-4V ELI powder (EOS, Krailling, Germany) using the laser powder bed fusion method (M290, EOS), which is a typical 3D printing technology. Using a powder with a particle size of 30 μm and laser focused to a diameter of approximately 80 μm, the designed structure shown in Fig. 1 was produced with high accuracy. The fabricated spacers were washed with acid to remove entrapped powder particles, followed by sterilization in an autoclave.

Sheep model and surgical procedure

Animal experiments were conducted in accordance with the Guidelines for the Proper Conduct of Animal Experiments of the Science Council of Japan. This study was approved by the Institutional Review Board of the Bioscience Department/Toya Laboratory of Hokudo Co., Ltd. (Hokkaido, Japan). Ten adult male Suffolk sheep (6.7± 2.6 years, weighing 55.6±6.3 kg) were used. The bleeding volume during surgery was recorded, and the health of the sheep post-operation was monitored. Under general anesthesia, a spacer was inserted using the right retroperitoneal approach as previously described [26]. The sheep were implanted with an experimental spacer with HTS (without autologous bone graft) and a control spacer (with autologous bone graft), which were randomly placed at the L2 −L3 or L4−L5 disc levels. Five spacers were tested for each group. An autologous bone graft was obtained from the right iliac crest of the same animal using a rongeur. After removing the cartilage tissues, the iliac crest bone was crushed with an electric bone mill (Midas Rex BM120; Medtronic, MN, USA) into bone fragments of 1 mm or smaller [27] and packed inside the control spacer. After spacer placement, a single screw/rod system consisting of 5-mm diameter screws (Kaneda SR, Depuy Synthes Spine, Raynham, MA, USA) was applied across L2−L3 and L4 −L5 to immediately stabilize the surgical sites. The incision was sutured and disinfected. The sheep were provided ad libitum access to food and tap water. At eight weeks after surgery, the sheep were euthanized by bolus intravenous injections of pentobarbital sodium, and the lumbar spines, including the spacers, were removed. The bone specimens were stored at -80°C until the push-out test was performed.

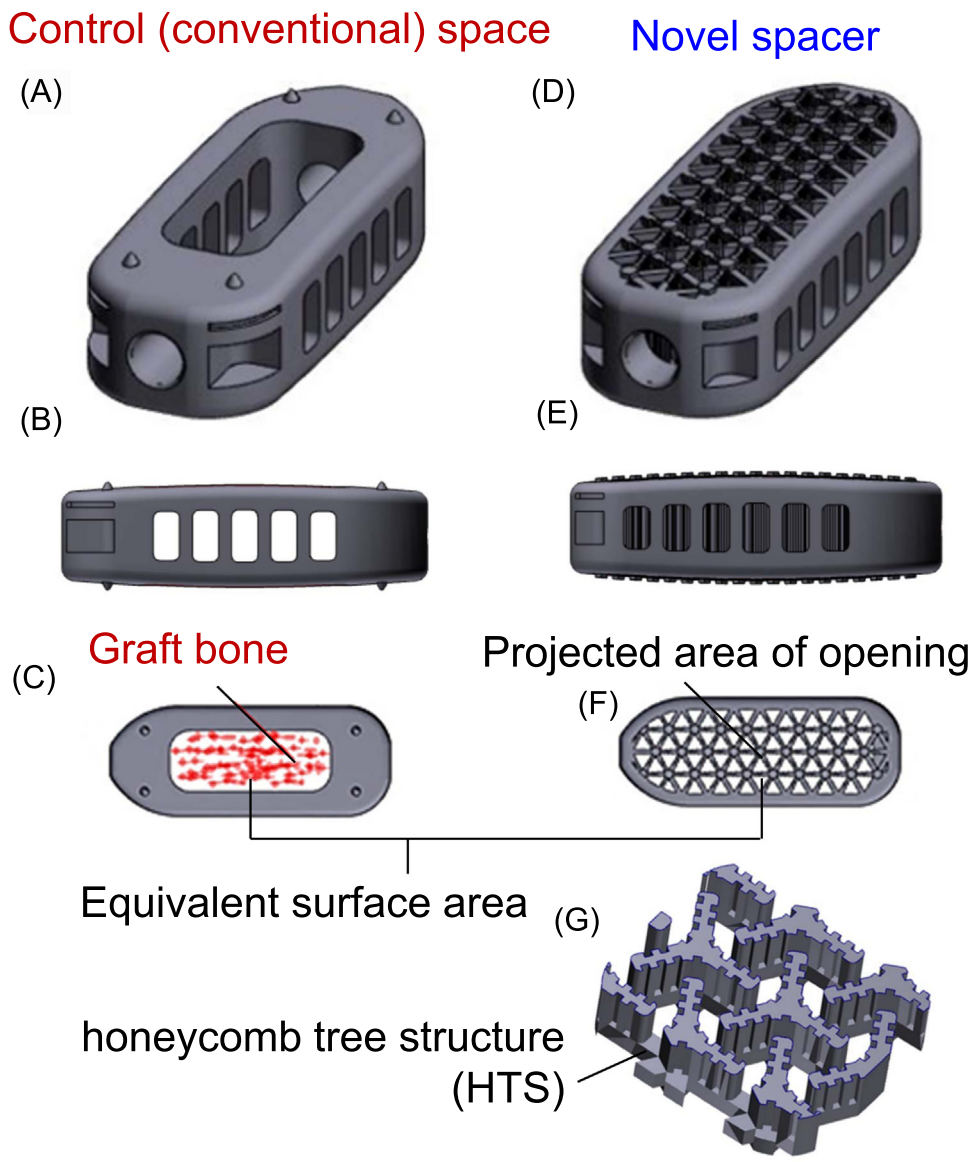

Fig. 1. (A) Control spacer with autologous bone graft and (D) novel spacer design with a through-pore with grooved substrate developed in this study. Model of the conventional spacer from the (B, E) sideview and (C, F) upperview. (G) Magnified schematic of the honeycomb tree structure (HTS) characterized by through-pore with grooved substrate.

Micro X-ray computed tomography

Micro-X-ray computed tomography (SMX-100CT, Shimadzu, Kyoto, Japan) was performed at 70 kV and 70 μA with a spatial resolution of 57 μm to nondestructively observe the spacer installation conditions.

Mechanical evaluation with the push-out test

A push-out test (Instron-5965; Instron, Norwood, MA, USA) was performed to evaluate the mechanical integrity of the spacer/bone interface [28]. The push-out test was performed at a crosshead speed of 5 mm/min until the spacer had completely exited the intervertebral space. The push-out spacer with the bone tissue inside and the remaining surrounding bone were immersed in 70% ethanol immediately after the test.

Specimen preparation

After the push-out test, the spacers and bone tissues were embedded in methyl methacrylate. Specimens of 500 and 100 μm thickness were sectioned along the dorsal plane at the center of the spacer.

Analysis of apatite c-axis orientation

The bone quality inside and outside the spacer was evaluated based on the orientation of the apatite *c*-axis using 500-μm-thick specimens, as described previously [24]. The preferential orientation of the apatite *c*-axis was analyzed

using a microbeam X-ray diffractometer equipped with a transmission optical system (R-Axis BQ; Rigaku, Tokyo, Japan). The incident beam (Mo-Kα) was generated at 50 kV and 90 mA collimated into a 200-μm circular spot and projected vertically onto each specimen. The 2D distribution of the apatite *c*-axis orientation along the surface of the thin specimens was analyzed. Diffracted X-rays were collected for 300 s using an imaging plate placed behind the specimens.

The (002) and (310) diffraction intensities of biological apatite were integrated along the azimuthal angle (β) based on the obtained Debye ring. The (002) represents the plane of the apatite *c*-axis, and the (310) was orthogonal to the (002). The intensity distributions of either (002) or (310) as a function of β for the diffraction intensities were individually fitted using the elliptic polynomial function [16]. The degree of the crystallographic texture of the apatite *c*-axis alignment was calculated as the intensity ratio of (002) to (310) for each β, resulting in a level of apatite *c*-axis orientation along the 2D plane vertical to the incident X-ray beam. The distribution of apatite orientation was visualized on a radar diagram, and the value on the cephalocaudal axis was analyzed.

Histology and quantitative analysis of collagen orientation

Undecalcified bone (100-μm-thick specimens) was stained with Villanueva Bone Stain. Histological and polarized images were obtained using an optical microscope (BX60; Olympus, Tokyo, Japan), and a birefringence imager (WPA-micro, Photonic Lattice, Miyagi, Japan) was used to evaluate the collagen orientation [14]. Collagen is a positive birefringent material, and the fast and slow axes indicate the orthogonal and parallel directions, respectively, to the long axis of the collagen fibers. The slow axis of a birefringent material means the axis in which the refraction index is higher. The slow-axis direction of the preferential collagen orientation was analyzed. Three polarized monochromatic lights with wavelengths of 523, 543, and 575 nm were used for birefringence analysis.

Statistical analyses

Quantitative results are expressed as the mean±standard deviation. Two-tailed paired *t*-test was used to compare data between the two groups. Statistical significance was set at $p<.05$.

Results

Spacer placement

Micro-X-ray computed tomography images of the sheep spines, including the spacer, at 8 weeks after implantation are shown in Fig. 2(A). The spacers were placed in the intervertebral spaces without rotation; therefore, the through-pores ran parallel to the cephalocaudal axis (Fig. 2 (B,C)). The grooves of the HTS were not clearly visible at this resolution. Bones inside the spacer could not be observed because of artifacts in the Ti-6Al-4V.

Mechanical integrity of the bone/spacer interface

The maximum load required to push the spacer out from the intervertebral spaces for each group is presented in Fig. 3(A). The strength at the bone/spacer interface of the novel spacer with an HTS was approximately three-fold greater compared with the control group ($p<.05$). Images of the spacers after the push-out tests are shown in Fig. 3(B). In the novel spacer, abundant bone tissue was observed in most pore openings. This finding indicates that new bone penetrated the HTS, and bone tissues inside and outside the spacer were interconnected. Based on its superior strength, the novel intervertebral spacer functionally fused the two

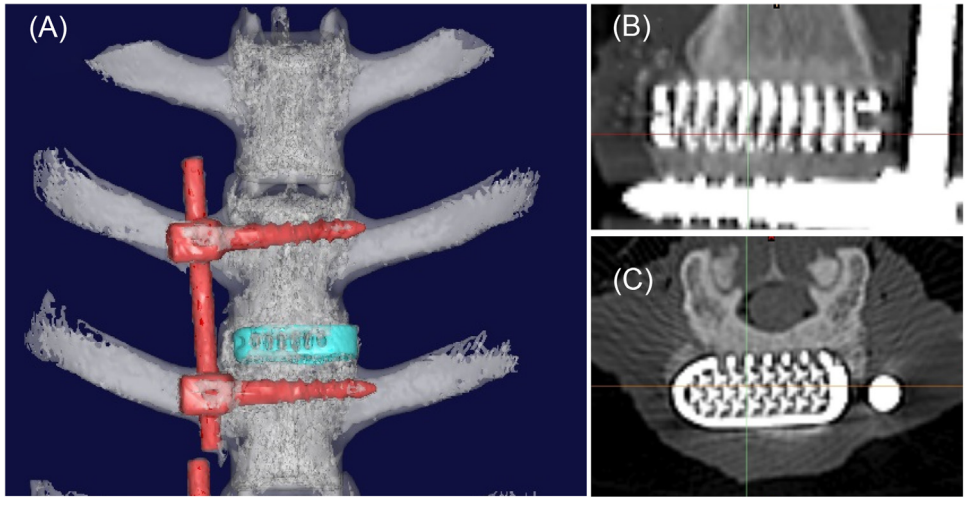

Fig. 2. Micro-X-ray computed tomography (μCT) images of sheep spines in (A) three-dimensional view, (B) transverse view, and (C) cross-sectional planes, including the spacer at eight weeks.

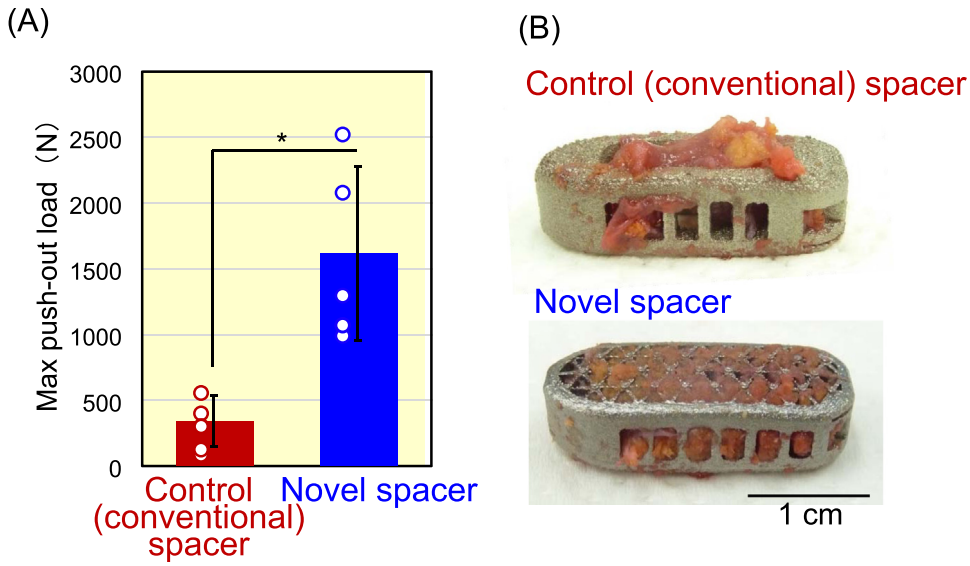

Fig. 3. Mechanical stability of the spacer/bone interface evaluated using a push-out test. (A) Variation in the push-out maximum load between the control and novel spacer groups. Data are shown in point clouds. *p<.05. (B) Images of spacers after the push-out test.

vertebrae to a greater extent than the conventional control spacer.

Bone ingrowth into the spacer

Typical histological images of the inside and surrounding spacers prepared after the push-out test are shown in Fig. 4. In each case, the surface of the spacer (bone/spacer interface) fractured during the push-out test (Fig. 4(A,C,F, H)). A large amount of bone was present inside the control spacer but most of this bone did not exhibit calcein fluorescence (Fig. 4(B)). The enlarged image (Fig. 4(D)) of the squared area indicates that the fragmented bones were scattered in a disordered manner, which significantly differed from the original vertebra shown in Fig. 4(E). In the control group, a significant amount of autogenous bone remained inside the spacer. Additionally, abundant calcein-labeled bone formation was observed inside the novel spacer

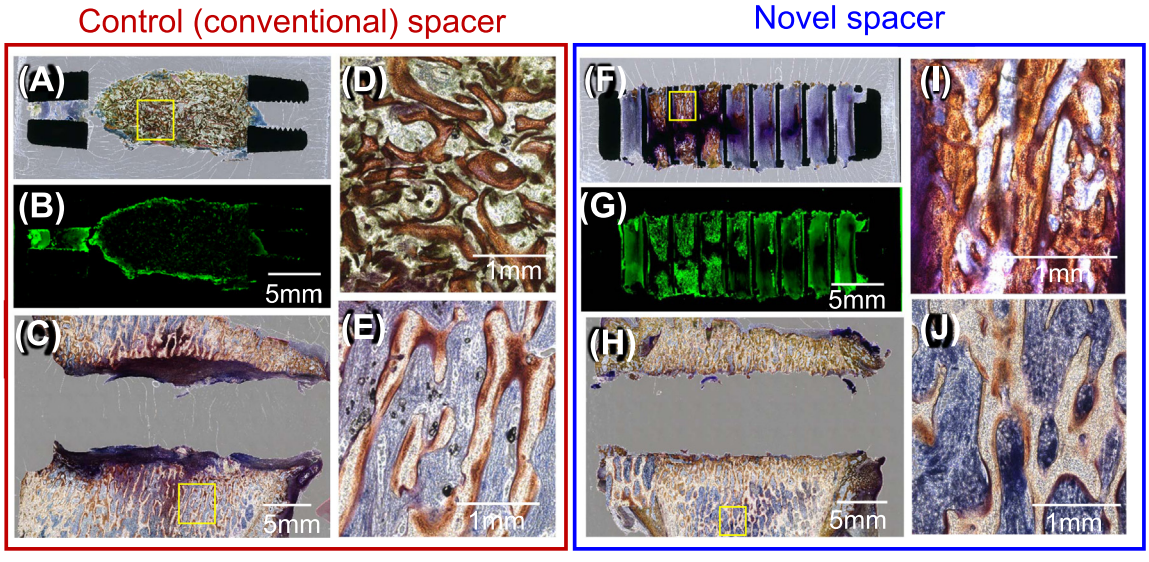

Fig. 4. Typical histological images of the areas inside and surrounding the spacer prepared after the push-out test. (A, B) Inside of the control spacer contained a large amount of bone, with minimal calcein fluorescence. (C) Surrounding tissue after the push-out test of control spacer. (D) Enlarged image of the squared region represents fragmented bones that are disorderly scattered, which differs from the (E) newly formed bone. (F,G) The trabecular-like bone resembling the normal trabecular bone penetrated from the ends of the novel spacer and showed calcein fluorescence. (H) Surrounding tissue after the push-out test of the novel spacer. (I) Enlarged image of the squared part represents anisotropic trabecular-like bone formation, which resembles the (J) normal trabecular bone.

(Fig. 4(G)). The enlarged image of the newly formed bone shows anisotropic trabecular-like bone mostly aligned along the cephalocaudal axis (Fig. 4(I)), resembling a normal trabecular bone (Fig. 4(J)).

Preferential orientation of collagen and apatite c-axis as a bone quality

Fig. 5(A) shows the optical and birefringence microscopy images obtained near the spacer surface. The bone in the control spacer (residual autogenous bone) showed a scattered orientation. In the novel spacer, trabecula-like bone invaded the center of the spacer along the metal wall, or HTS, which was parallel to the cephalocaudal axis. The birefringence images that ordered collagen fibers formed and were interconnected through the interface between the novel spacer and bone (Fig. 5(A)). The quantitative distribution of the degrees of collagen fiber orientation and apatite *c*-axis alignment inside and outside the spacer along the cephalocaudal axis are shown in Figs. 5(C) and 6, respectively. Measurements were taken at distances of up to 3 mm outward (minus side) and inward (plus side) from the spacer surface, and statistical analyses were performed at positions -1, -0.5, 0, +1, and +2 mm (Fig. 5(B)). The collagen and apatite orientations were quantitatively determined by measuring the distance from the bone/spacer interface. The data in Figs. 5(C) and 6 show the collagen and apatite orientations depending on the distance from the device surface, respectively. Each data plot in Fig. 7 corresponds to the data in Figs. 5(C) and 6 (outside of the novel spacer: 9 points, inside of the novel spacer; 8 points, outside of the control spacer; 8 points, inside of the control spacer; 8 points, including 4 points as remaining graft bone). As shown in Fig. 7, the apatite and collagen orientations showed strong, positive, and significant correlations, respectively, indicating that the apatite crystallized epitaxially on the collagen template such that its crystallographic *c*-axis was parallel to the elongated direction of the collagen fiber.

The collagen and apatite orientation inside the control spacer was significantly low. Moreover, the collagen and apatite orientation along the cephalocaudal axis was significantly reduced on the outer side of the spacer to less than 1 mm from the spacer surface. In contrast, in the novel spacer, the degree of the apatite orientation along the cephalocaudal axis of the regenerated bone inside the spacer was comparable to that of normal trabecular bone. Importantly, the apatite orientation was not scattered even near the spacer surface. Collagen and apatite were preferentially oriented along the cephalocaudal axis within the trabecula,

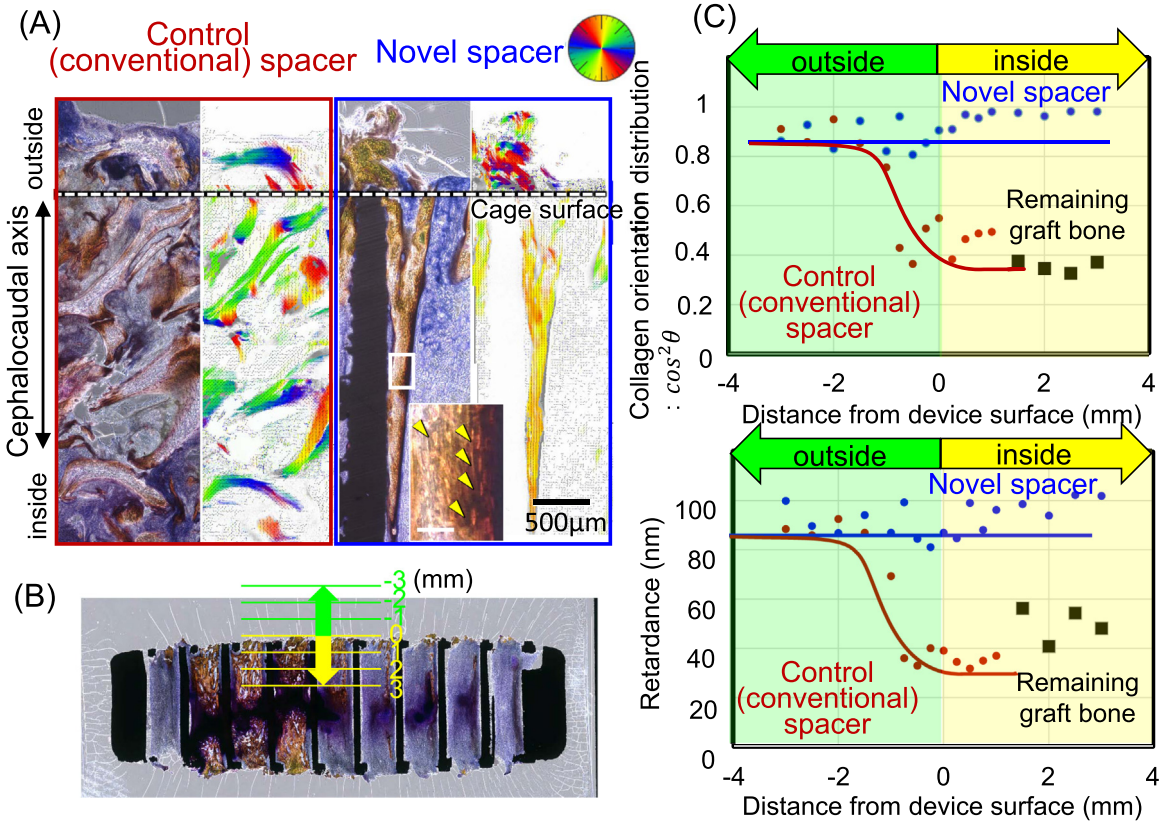

Fig. 5. (A) Histological evaluation and collagen orientation distribution in areas inside and surrounding the spacer. (Left) Typical Villanueva bone staining images, and (Right) birefringence images at 8 weeks post-implantation. Inset shows osteocytes in the new bone aligned parallel to the groove direction, with many canaliculi laying orthogonal to the principal stress. (B) Selected analysis region from the outside of the spacer to the inside, indicating the distance from the device surface. (C) Distribution of the running direction and retardance of the collagen matrix inside and outside of the spacer.

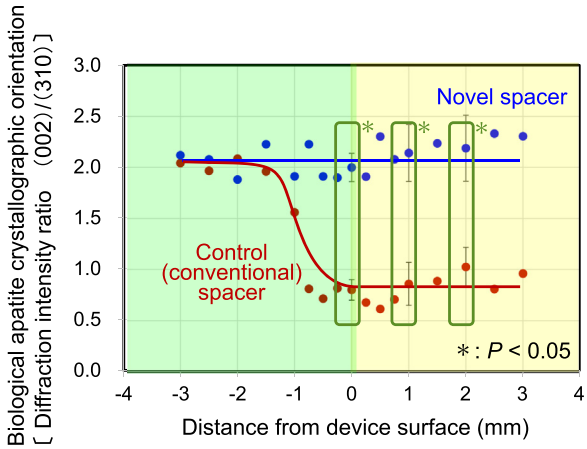

Fig. 6. Distribution of the degree of preferential apatite *c*-axis orientation along the cephalocaudal axis inside and outside of the spacer at 8 weeks post-implantation. *p<.05.

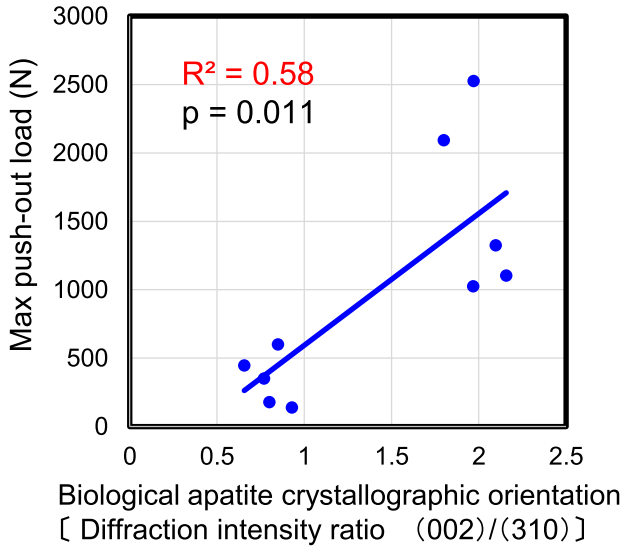

Fig. 8. Correlation between the push-out load and degree of apatite orientation along the cephalocaudal direction. The push-out load was positively correlated with the degree of apatite orientation.

demonstrating induction of the new bone mimicking native trabecular bone with an anisotropic trabecula-like macroscopic structure and collagen and apatite orientation at the nanoscale inside the novel spacer at 8 weeks after spacer implantation.

Factors determining bone/spacer interfacial strength

The correlation between the push-out load and degree of apatite orientation along the cephalocaudal direction is shown in Fig. 8. The push-out load was positively correlated with the degree of apatite orientation (R^2=0.58, p<.05). Thus, the bone/spacer interfacial strength was governed by the apatite orientation, supporting that our design strategy can induce bone to develop a highly oriented collagen and apatite microstructure.

Discussion

An intervertebral spacer with an HTS was designed and developed, which formed an intact bone-like hierarchically anisotropic trabecular structure with a macroscopic trabecular architecture and collagen and apatite orientation at the nanometer scale. Our novel intervertebral spacer enabled functional fusion of two adjacent vertebrae by organizing a new trabecular-like bone with a highly oriented collagen and apatite alignment along the cephalocaudal axis, to which principal stress was applied.

Autologous iliac crest bone grafts are the gold standard in spinal surgery. Autologous bone grafts are used because of their osteogenic, osteoinductive, and osteoconductive potential and are predominantly derived from bone marrow

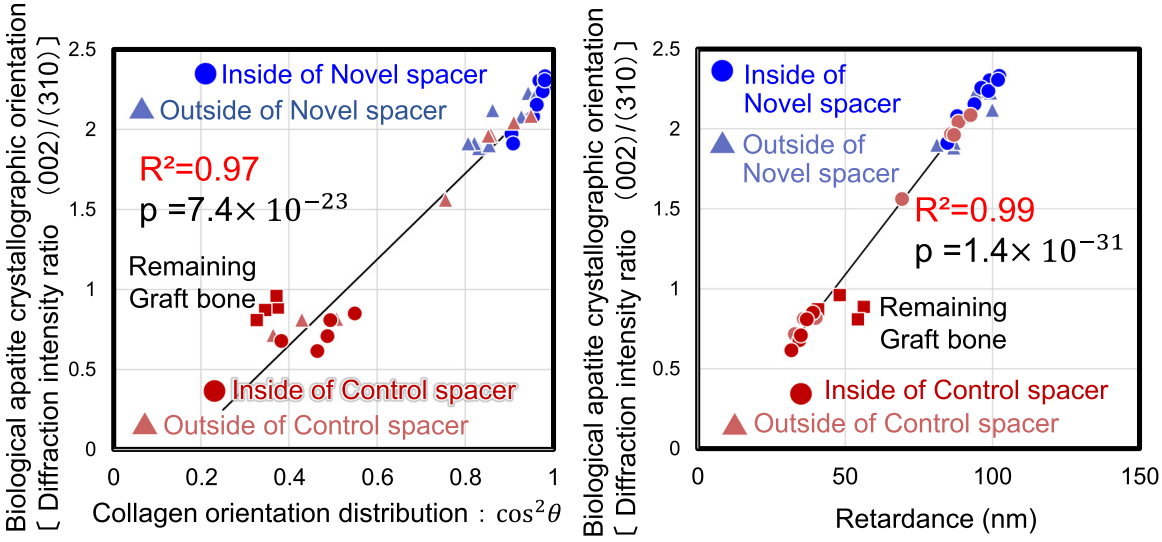

Fig. 7. Collagen orientation and apatite alignment showed a strong, positive, and significant correlation.

containing abundant viable bone marrow cells [29]. However, in the present study, the spacer/bone interface strength of the box-type spacer with autologous bone graft was significantly inferior to that of the novel spacer at eight weeks after implantation. Autologous bone did not promote osteogenesis, remained inside the spacer even at eight weeks after implantation, and appeared to interfere with bone formation inside the spacer. The properties of the bone at the spacer/bone interface are important for the bone's connection strength and thus the mechanical stability of the spacer. In the control spacer with an autogenous bone graft, the degree of collagen and apatite orientation along the cephalocaudal axis around the spacer/bone interface was significantly lower compared with the novel spacer. Notably, the collagen and apatite orientation along the cephalocaudal axis was largely scattered within 1 mm of the outer side of the spacer. Therefore, at least in the early stages of implantation, autogenous bone may negatively affect the surrounding bone, thus delaying mechanical stabilization of the spacer. The long-term outcomes of spinal spacer instrumentation have been widely evaluated, particularly in clinical studies. Our results indicate that spacer instability in the early stages of implantation must be further investigated to verify the advantages and disadvantages of autologous bone grafting.

These results are clinically relevant, as the novel spacer with an HTS induced the formation of high-quality new bone with high bone/spacer interface strength at eight weeks post-implantation, indicating functional fusion between the two vertebrae via the intervertebral spacer. The HTS shows potential for replacing autologous bone grafts, as bone formation occurred directly on the HTS surface, avoiding the bone resorption phase during which bone formation is inhibited. Thus, accelerated guidance of the bone matrix orientation of collagen and apatite can be achieved using the HTS. The proposed intervertebral spacer with an HTS can overcome the limitations of innate regeneration of the oriented bone matrix microstructure, as shown in Fig. 9. The HTS allows for immediate texture formation of the regenerated bone matrix, which cannot occur during the innate recovery process. Mature regeneration of the anisotropic bone matrix enables stress transmission from the host bone, resulting in the formation of fully functionalized vertebrae. Osteoblast extension and alignment is one factor leading to the generation of an oriented collagen and apatite microstructure [18,19], which can be induced by an anisotropic topology with optimal dimensions in the substrate plane [30,31]. Collagen produced by aligned osteoblasts is preferentially aligned parallel to the cell body extension based on the interface mechanical reaction between myosin II and the cell-produced matrix assembly [23,32]. Osteoblasts have been reported to align on the substrate grooves fabricated using laser powder bed fusion [24]. Although we could not directly observe the alignment of osteoblasts on the HTS in vivo, collagen and apatite may have been oriented in the groove direction when osteoblasts were stretched and aligned by the groove on the HTS. The fact that osteocytes in new bone are aligned parallel to the groove direction supports that osteoblasts are also aligned in the groove. In addition, the through-pore of the HTS extending in the same direction as the groove allowed for the growth of trabecular bone in the direction of the pore, resulting in a multiscale anisotropic structure in which the macroscopic trabecular architecture and collagen and apatite orientation

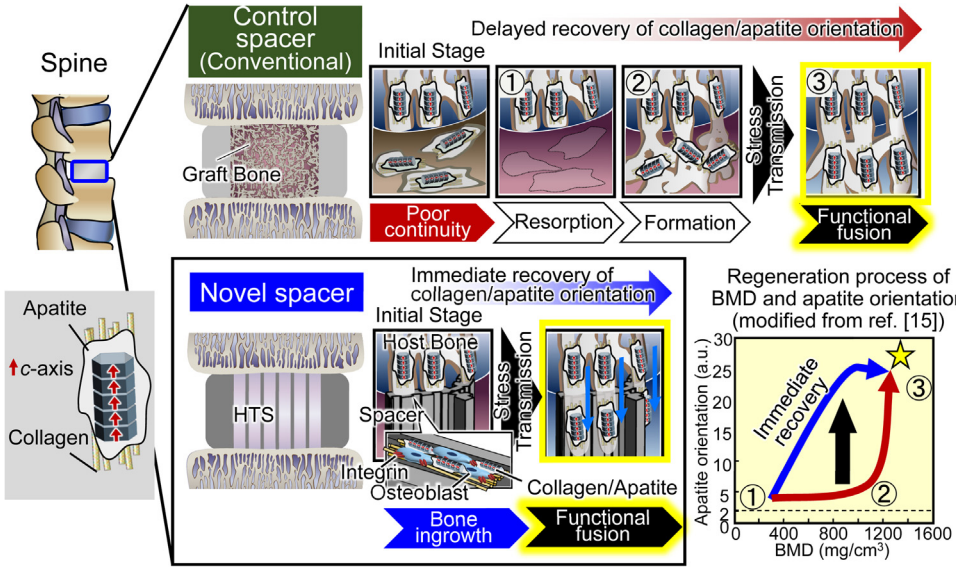

Fig. 9. Schematic illustration of the potential advantage of the novel spacer, which guides bones with anisotropic collagen and apatite orientation in the through-pore and groove direction, resulting in stabilized vertebrae immobilization. HTS overcomes the limitation of textural recovery in innate bone regeneration and ensures mechanosensory function, thus enabling the maintenance of long-term bone health.

(anisotropic arrangement) inside the trabecula were superimposed. This multiscale anisotropic structure is characteristic of functional vertebral trabeculae [17].

The arrangement of osteocytes along the groove direction (cephalocaudal axis) is directly related to the mechanosensory function of these cells. Osteocytes are thought to sense mechanical stimuli towards bone based on fluid flow inside the canaliculi [33,34], which is known as the fluid flow theory. Elongated osteocytes have canaliculi that preferentially align perpendicularly to the elongated direction of the cell body [35]. Stress is thought to be an important factor controlling the collagen and apatite orientation in bone, and the stimulation of osteocytes, as mechanosensory cells, by stress-induced strain of the bone matrix is involved in the formation of oriented collagen and apatite microstructures [36]. Osteocytes elongated parallel to the cephalocaudal axis, to which the principal stress is applied, have many canaliculi that are orthogonal to the principal stress. These canaliculi are efficiently collapsed by matrix strain generated by stress and thus are suitable for stress sensing based on fluid flow inside the canaliculi [35]. The bone formed inside the novel spacer exhibited mechanosensory function, thus enabling the maintenance of long-term bone health. This is a powerful advantage of the novel spacer, which can artificially control osteocyte mechanosensory functions during the long-term implantation period.

This study is limited by the lack of bone density data before the operation, as it is difficult to noninvasively measure bone density in large animal models. Additionally, we did not evaluate the long-term outcomes of novel cage implantation into the intervertebral space. An important issue is the stress shielding arising from differences in the elastic modulus between the bone and implant. Examination after a longer period to detect fusion, such as at 28 weeks after implantation, should be performed. Designing and fabricating the device using β-type titanium alloys with a bone-mimetic low Young's modulus help resolve these issues [37]. To overcome these limitations, the desired crystallographic texture can be obtained by controlling the scanning and fabrication strategy during metal 3D printing [38]. The structural and material properties can be controlled to produce a device with the required functions. Furthermore, to achieve the biofamiliar 3D-architectural nature of the organ that can change over time in response to external stimuli throughout regeneration, advanced 4D-printed medical devices can be produced based on our results.

Conclusion

A novel intervertebral spacer targeting to produce bone of high quality with a through-pore grooved structure (HTS) was developed. The novel spacer forms an anisotropic collagen and apatite matrix microstructure along the through-pore and groove directions, resulting in stabilized immobilization between the host bone and spacer. In contrast to autologous bone, which tends to delay bone maturation because of the need for resorption before bone formation, the HTS in the spacer provided a direct scaffold that guided the bone matrix in the collagen and apatite orientation, enabling functional spinal fusion from an early stage of implantation. Notably, the spacer exhibited substantially greater strength at the spacer/host bone interface compared with that of conventional and gold-standard box-type spacers with autologous iliac bone grafts. This concept will enable the design of highly functionalized spinal devices that can be applied in clinical settings.

Authors' contributions

Aira Matsugaki: Acquisition and data, Analysis and interpretation of data, Drafting of the manuscript, Statistical analysis. *Manabu Ito:* Conception and design (animal study), Analysis and interpretation of data, Critical revision of the manuscript for important intellectual content. *Yoshiya Kobayashi:* Acquisition and data, Analysis and interpretation of data, Statistical analysis. *Tadaaki Matsuzaka:* Acquisition and data, Analysis and interpretation of data. *Ryosuke Ozasa:* Acquisition and data, Analysis and interpretation of data. *Takuya Ishimoto:* Acquisition and data, Analysis and interpretation of data, Drafting of the manuscript, Statistical analysis. *Hiroyuki Takahashi:* Acquisition and data, Analysis and interpretation of data, Critical revision of the manuscript for important intellectual content. *Ryota Watanabe:* Acquisition and data, Analysis and interpretation of data. *Takayuki Inoue:* Acquisition and data, Analysis and interpretation of data. *Katsuhiko Yokota:* Supervision. *Yoshio Nakashima:* Supervision. *Takashi Kaito:* Acquisition and data, Analysis and interpretation of data. *Seiji Okada:* Acquisition and data, Analysis and interpretation of data. *Takao Hanawa:* Supervision. *Yukihiro Matsuyama:* Acquisition and data, Analysis and interpretation of data. *Morio Matsumoto:* Acquisition and data, Analysis and interpretation of data. *Hiroshi Taneichi:* Acquisition and data, Analysis and interpretation of data. *Takayoshi Nakano:* Conception and design (all study containing the spacer design), Analysis and interpretation of data, Obtaining funding, Supervision.

Acknowledgment

This study was supported by Grants-in-Aid for Scientific Research (JP18H05254) from the Japan Society for the Promotion of Science (JSPS) and the Strategic Promotion of Innovative Research and Development (S-Innovation) from the Japan Agency for Medical Research and Development (AMED), The grant number is JPMJSV1212.

Declaration of competing interest

Manabu Ito is the chairperson of the AOSpine Asia Pacific. The other authors declare that they have no conflict of interest.

References

[1] Sen MK, Miclau T. Autologous iliac crest bone graft: should it still be the gold standard for treating nonunions? Injury 2007;38(Suppl. 1): S75–80. https://doi.org/10.1016/j.injury.2007.02.012.

[2] Aghdasi B, Montgomery SR, Daubs MD, Wang JC. A review of demineralized bone matrices for spinal fusion: the evidence for efficacy. Surgeon 2013;11:39–48. https://doi.org/10.1016/j.surge.2012.08.001.

[3] Rihn JA, Kirkpatrick K, Albert TJ. Graft options in posterolateral and posterior interbody lumbar fusion. Spine 2010;35:1629–39. https://doi.org/10.1097/BRS.0b013e3181d25803.

[4] Christy PN, Basha SK, Kumari VS, Bashir AKH, Maaza M, Kaviyarasu K, et al. Biopolymeric nanocomposite scaffolds for bone tissue engineering applications − a review. J Drug Deliv Sci Technol 2020;55:101452. https://doi.org/10.1016/j.jddst.2019.101452.

[5] Ishimoto T, Yamada K, Takahashi H, Takahata M, Ito M, Hanawa T, et al. Trabecular health of vertebrae based on anisotropy in trabecular architecture and collagen/apatite micro-arrangement after implantation of intervertebral fusion cages in the sheep spine. Bone 2018;108:25–33. https://doi.org/10.1016/j.bone.2017.12.012.

[6] Miyabe S, Nakano T, Ishimoto T, Takano N, Adachi T, Iwaki H, et al. Two-dimensional quantitative analysis of preferential alignment of BAp c-axis for isolated human trabecular bone using microbeam X-ray diffractometer with a transmission optical system. Mater Trans 2007;48:343–7. https://doi.org/10.2320/matertrans.48.343.

[7] Landis WJ. The strength of a calcified tissue depends in part on the molecular structure and organization of its constituent mineral crystals in their organic matrix. Bone 1995;16:533–44. https://doi.org/10.1016/8756-3282(95)00076-P.

[8] Nakano T, Kaibara K, Tabata Y, Nagata N, Enomoto S, Marukawa E, et al. Unique alignment and texture of biological apatite crystallites in typical calcified tissues analyzed by microbeam X-ray diffractometer system. Bone 2002;31:479–87. https://doi.org/10.1016/S8756-3282(02)00850-5.

[9] Nakano T, Kaibara K, Ishimoto T, Tabata Y, Umakoshi Y. Biological apatite (BAp) crystallographic orientation and texture as a new index for assessing the microstructure and function of bone regenerated by tissue engineering. Bone 2012;51:741–7. https://doi.org/10.1016/j.bone.2012.07.003.

[10] Wang J, Ishimoto T, Nakano T. Unloading-induced degradation of the anisotropic arrangement of collagen/apatite in rat femurs. Calcif Tissue Int 2017;100:87–94. https://doi.org/10.1007/s00223-016-0200-0.

[11] Ozasa R, Matsugaki A, Ishimoto T, Kamura S, Yoshida H, Magi M, et al. Bone fragility via degradation of bone quality featured by collagen/apatite micro-arrangement in human rheumatic arthritis. Bone 2022;155:116261. https://doi.org/10.1016/j.bone.2021.116261.

[12] Ozasa R, Ishimoto T, Miyabe S, Hashimoto J, Hirao M, Yoshikawa H, et al. Osteoporosis changes collagen/apatite orientation and Young's modulus in vertebral cortical bone of rat. Calcif Tissue Int 2019;104:449–60. https://doi.org/10.1007/s00223-018-0508-z.

[13] Sekita A, Matsugaki A, Ishimoto T, Nakano T. Synchronous disruption of anisotropic arrangement of the osteocyte network and collagen/apatite in melanoma bone metastasis. J Struct Biol 2017;197:260–70. https://doi.org/10.1016/j.jsb.2016.12.003.

[14] Sekita A, Matsugaki A, Nakano T. Disruption of collagen/apatite alignment impairs bone mechanical function in osteoblastic metastasis induced by prostate cancer. Bone 2017;97:83–93. https://doi.org/10.1016/j.bone.2017.01.004.

[15] Ishimoto T, Nakano T, Umakoshi Y, Yamamoto M, Tabata Y. Degree of biological apatite c-axis orientation rather than bone mineral density controls mechanical function in bone regenerated using recombinant bone morphogenetic protein-2. J Bone Miner Res 2013;28:1170–9. https://doi.org/10.1002/jbmr.1825.

[16] Noyama Y, Nakano T, Ishimoto T, Sakai T, Yoshikawa H. Design and optimization of the oriented groove on the hip implant surface to promote bone microstructure integrity. Bone 2013;52:659–67. https://doi.org/10.1016/j.bone.2012.11.005.

[17] Auger JD, Frings N, Wu Y, Marty AG, Morgan EF. Trabecular architecture and mechanical heterogeneity effects on vertebral body strength. Curr Osteoporos Rep 2020;18:716–26. https://doi.org/10.1007/s11914-020-00640-0.

[18] Matsugaki A, Isobe Y, Saku T, Nakano T. Quantitative regulation of bone-mimetic, oriented collagen/apatite matrix structure depends on the degree of osteoblast alignment on oriented collagen substrates. J Biomed Mater Res A 2015;103:489–99. https://doi.org/10.1002/jbm.a.35189.

[19] Matsugaki A, Aramoto G, Nakano T. The alignment of MC3T3-E1 osteoblasts on steps of slip traces introduced by dislocation motion. Biomaterials 2012;33:7327–35. https://doi.org/10.1016/j.biomaterials.2012.06.022.

[20] Matsugaki A, Fujiwara N, Nakano T. Continuous cyclic stretch induces osteoblast alignment and formation of anisotropic collagen fiber matrix. Acta Biomater 2013;9:7227–35. https://doi.org/10.1016/j.actbio.2013.03.015.

[21] Matsugaki A, Aramoto G, Ninomiya T, Sawada H, Hata S, Nakano T. Abnormal arrangement of a collagen/apatite extracellular matrix orthogonal to osteoblast alignment is constructed by a nanoscale periodic surface structure. Biomaterials 2015;37:134–43. https://doi.org/10.1016/j.biomaterials.2014.10.025.

[22] Nakanishi Y, Matsugaki A, Kawahara K, Ninomiya T, Sawada H, Nakano T. Unique arrangement of bone matrix orthogonal to osteoblast alignment controlled by Tspan11-mediated focal adhesion assembly. Biomaterials 2019;209:103–10. https://doi.org/10.1016/j.biomaterials.2019.04.016.

[23] Kalson NS, Starborg T, Lu Y, Mironov A, Humphries SM, Holmes DF, et al. Nonmuscle myosin II powered transport of newly formed collagen fibrils at the plasma membrane. Proc Natl Acad Sci USA 2013;110:E4743–52. https://doi.org/10.1073/pnas.1314348110.

[24] Ishimoto T, Kobayashi Y, Takahata M, Ito M, Matsugaki A, Takahashi H, et al. Outstanding in vivo mechanical integrity of additively manufactured spinal cages with a novel "honeycomb tree structure" design via guiding bone matrix orientation. Spine J 2022;22:1742–7. https://doi.org/10.1016/j.spinee.2022.05.006.

[25] Grunhagen T, Wilde G, Soukane DM, Shirazi-Adl SA, Urban JP. Nutrient supply and intervertebral disc metabolism. J Bone Joint Surg Am 2006;88:30–5. https://doi.org/10.2106/JBJS.E.01290.

[26] Ito M, Kotani Y, Hojo Y, Abumi K, Kadosawa T, Minami A. Evaluation of hydroxy apatite ceramic vertebral spacers with different porosities and their binding capability to the vertebral body: an experimental study in sheep. J Neurosurg Spine 2007;6:431–7. https://doi.org/10.3171/spi.2007.6.5.431.

[27] Pelletier MH, Cordaro PVM, Waites M, Lau A, Walsh WR. PEEK versus Ti interbody fusion devices, resultant fusion, bone apposition, initial and 26-week biomechanics. Clin Spine Surg 2016;29:208–14. https://doi.org/10.1097/BSD.0b013e31826851a4.

[28] Guyer RD, Abitbol JJ, Ohnmeiss DD, Yao C. Evaluating osseointegration into a deeply porous titanium scaffold: a biomechanical comparison with PEEK and allograft. Spine 2016;41:E1146–50. https://doi.org/10.1097/BRS.0000000000001672.

[29] Li H, Zou X, Xue Q, Egund N, Lind M, Bünger C. Effects of autogenous bone graft impaction and tricalcium phosphate on anterior interbody fusion in the porcine lumbar spine. Acta Orthop Scand 2004;75:456–63. https://doi.org/10.1080/00016470410001240-1.

[30] Wu L, Lee LA, Niu Z, Ghoshroy S, Wang Q. Visualizing cell extracellular matrix (ECM) deposited by cells cultured on aligned bacteriophage M13 thin films. Langmuir 2011;27:9490–6. https://doi.org/10.1021/la201580v.

[31] Guillemette MD, Cui B, Roy E, Gauvin R, Giasson CJ, Esch MB, et al. Surface topography induces 3D self-orientation of cells and

extracellular matrix resulting in improved tissue function. Integr Biol (Camb) 2009;1:196–204. https://doi.org/10.1039/b820208g.

[32] Canty EG, Lu Y, Meadows RS, Shaw MK, Holmes DF, Kadler KE. Coalignment of plasma membrane channels and protrusions (fibripositors) specifies the parallelism of tendon. J Cell Biol 2004;165:553–63. https://doi.org/10.1083/jcb.200312071.

[33] Burger EH, Klein-Nulend J. Mechanotransduction in bone − role of the lacuno-canalicular network. FASEB J 1999;13:S101–12. https://doi.org/10.1096/fasebj.13.9001.s101.

[34] Bonewald LF. The amazing osteocyte. J Bone Miner Res 2011;26:229–38. https://doi.org/10.1002/jbmr.320.

[35] Ishimoto T, Kawahara K, Matsugaki A, Kamioka H, Nakano T. Quantitative evaluation of osteocyte morphology and bone anisotropic extracellular matrix in rat femur. Calcif Tissue Int 2021;109:434–44. https://doi.org/10.1007/s00223-021-00852-1.

[36] Matsuzaka T, Matsugaki A, Nakano T. Control of osteoblast arrangement by osteocyte mechanoresponse through prostaglandin E2 signaling under oscillatory fluid flow stimuli. Biomaterials 2021;279:121203. https://doi.org/10.1016/j.biomaterials.2021.121203.

[37] Lee SH, Todai M, Tane M, Hagihara K, Nakajima H, Nakano T. Biocompatible low Young's modulus achieved by strong crystallographic elastic anisotropy in Ti-15Mo-5Zr-3Al alloy single crystal. J Mech Behav Biomed Mater 2012;14:48–54. https://doi.org/10.1016/j.jmbbm.2012.05.005.

[38] Ishimoto T, Hagihara K, Hisamoto K, Sun SH, Nakano T. Crystallographic texture control of beta-type Ti-15Mo-5Zr-3Al alloy by selective laser melting for the development of novel implants with a biocompatible low Young's modulus. Scr Mater 2017;132:34–8. https://doi.org/10.1016/j.scriptamat.2016.12.038.